Chapter 8

Holographic Printing of White-Light Viewable Holograms and Stereograms

Hoonjong Kang, Elena Stoykova, Jiyung Park,
Sunghee Hong and Youngmin Kim

Additional information is available at the end of the chapter

http://dx.doi.org/10.5772/53412

1. Introduction

Denis Gabor [1] invented the holographic method to improve the resolution of an electron microscope in 1948. Following the invention of the coherent light sources a decade later, the holographic techniques proved their unique potential in many fields as three-dimensional (3D) display technology [2], optical metrology [3], medicine [4], commerce etc. Among them, full-color and full parallax high resolution holographic printing as a technique for recording of 3D objects and scenes which are reconstructed under white light illumination is experiencing extensive development. The holographic printing, being a part of the research on 3D imaging of 3D objects from sampled data sets by holographic means, also followed the two main approaches in this area: i) computation of the holographic fringes by numerical simulation of the interference and encoding the resulting pattern onto a suitable medium for further optical display; ii) digital acquisition or computation of a set of discrete perspectives of a scene and their optical multiplexing in a holographic medium for building a stereoscopic pseudo 3D image.

A holographic stereogram (HS) has received much research attention since it can reduce the bandwidth of the hologram by defining a viewing scope, while the holography is a technique to reconstruct the real wavefront of the light field coming from the object. That's why the HSs form a separate region in the field of holographic printing. However, more studies of this innovative method had to be navigated because of the inherent characteristics of holographic recording. A two-step method, spatially-multiplexing technique, horizontal-parallax-only (HPO) method, and HS' exposure geometry were instances of such valuable efforts. Figure 1 shows the historical events of the important technical developments related to the HS.

The early experiment on a HS was conducted by R. V. Pole in 1967. Pole's experiment included recording of multiple perspectives by means of two-dimensional (2D) fly's eye lenslet array

with incoherent white light, and then transfer of the perspectives onto the holographic material [5]. De Bitetto's spatially-multiplexed technique via sequential exposure of a fine grain film (such as Panatomic-X) provided a clue to overcome the resolution limitation of Pole's original approach to the HS [6]. The intensive research on printing HSs had been conducting since 1970s [7]. In [7], a large HS was recorded from a sequence of computed perspective images of a 3D object taken from multiple viewpoints equidistantly placed on a part of a circle. Benton's "Rainbow" hologram [8] and Lloyd Cross's "Multiplex(TM)" [9], which were developed with a HPO holographic technique, were the expression of the efforts for the reduction of the bandwidth and the simple acquisition of perspective images.

In 1974, Yatagai [10, 11] proposed a method to accelerate producing of computer-generated HSs. According to this method, computer calculated not only the perspective images but also the elemental hologram through Fourier transform of these images to build the composite hologram. The research was pushed forward in 1990 for a straightforward process with the help of a spatial light modulator (SLM) and the introduction of a pulsed laser, when an one-step printer for full parallax holographic stereograms was invented [12, 13]. The essence of the method was successive recording of multiple volume-type elemental holograms by displaying on a SLM the angular distribution of the light field for each elemental hologram built from a sequence of perspective 2D images. The result is a stereoscopic vision at a varying viewing angle. In 1998 a holographic printer for one-step color full parallax HSs was patented [14], which was further improved by Geola group [15-17] by proposing much faster and more stable pulsed RGB lasers implementation of the holoprinting technique. Nowadays the advanced HS printers with CW or pulse laser illumination can produce white-light viewable large format digital color holograms [18]. Recently, promising results have been reported when the holographic stereogram technique was applied to realize a quasi-real-time 3D display by printing on a newly developed erasable dynamic photorefractive material [19] by using pulsed lasers illumination. The principle of the HS was implemented in a curved array dynamic holographic display built from many SLMs [20].

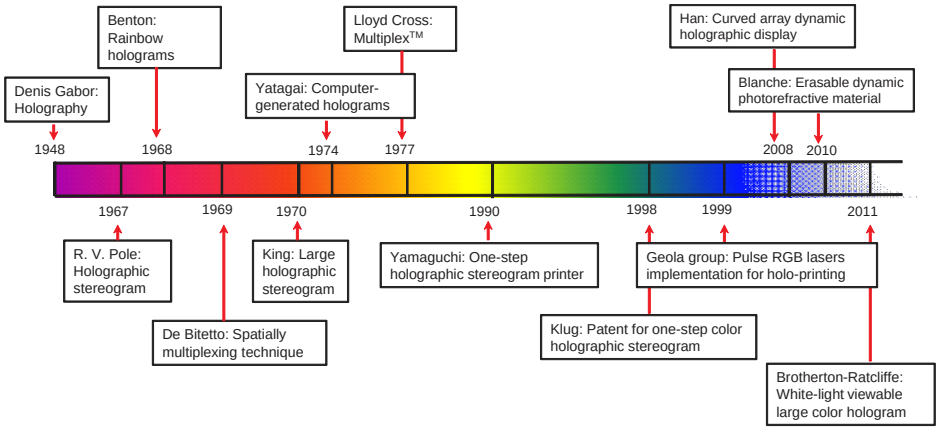

Figure 1. Historical events of the technical developments for a holographic stereogram.

http://dx.doi.org/10.5772/53412

In 2004, a device for direct printing of the holographic fringe pattern was proposed and developed [21, 22]. The holographic fringe pattern is computer generated from the 3D information extracted from a 3D object and further printed onto a photo-sensitive holographic plate. The SLM displays in this case a fractional part of the fringe pattern for recording an elemental hologram. Since then a lot of efforts have been focused on direct printing of various types of computer generated holograms which can be reconstructed under laser or white-light illumination.

The structure of the Chapter is as follows: **Section 2**, which consists of five subsections, gives a critical analysis of the research on printing HSs and a survey of the recent achievements in printing large-format full-color HSs. **Subsection 2.1** describes the principle of the HS printing. **Subsection 2.2** considers advantages and drawbacks of different methods for acquisition of perspective images and explains forming of the parallax related images. **Subsection 2.3** provides analysis of distortions which worsen the quality of the reconstructed image. **Subsection 2.4** presents a simulation tool developed by us for numerical reconstruction of the HS from the formed parallax images as a quality check before printing. **Subsection 2.5** presents the main blocks of the printer set-up and describes the main requirements set on the photo-sensitive materials used for panchromatic holographic recording of volume reflection holograms. **Section 3** consists of three subsections and is dedicated to direct printing of a holographic fringe pattern on a photo-sensitive material. **Subsection 3.1** introduces briefly the dedicated acceleration methods for generation of fringe patterns for various holograms which can be manufactured by holographic printing techniques. Furthermore, **Subsection 3.2** focuses on the technique for direct printing of the generated holographic fringe pattern onto the holographic emulsion. **Subsection 3.3** treats a wave-front recording technique which is novel technology. The essence of the method is to record as a volume hologram the wave field diffracted from a holographic fringe pattern displayed on a suitable SLM. As a result, a digitally designed volume hologram is recorded whose quality is comparable to a conventional analog hologram. The conclusion of the Chapter gives the future trends in the holographic printing.

2. Printing of holographic stereograms

2.1. Holographic stereograms — Principle of the holographic printing

Holographic stereograms are popular autostereoscopic display devices with a strong visual impact [23]. They implement the idea of displaying a 3D scene by using stereo-images and the property of the holographic medium to record 3D wavefront through interference and to reconstruct it by diffraction. The underlying technology behind the HS stems from the off-axis display holography and the autostereoscopic approaches in lenticular and parallax barrier displays [24]. This technology allows high-quality quasi-holographic 3D imaging of large objects. To make a HS, a sequence of 2D images of the scene is incoherently acquired from multiple views. The directional information carried by these perspective images is processed to form parallax-related images which after displaying on a projection screen are recorded onto a holographic photo-sensitive material by a coherent source in a two-beam recording

scheme. The parallax-related images modulate the intensity of the object beam. The whole hologram is divided into elemental holograms which are sequentially exposed to the parallax-related images. Illumination of the fringe pattern recorded in the hologram for reconstruction of the 3D scene ensures spatial multiplexing of the perspective views.

Stereoscopy reduces substantially the huge amount of information encoded in a hologram, since this information is recorded from a finite discrete set of viewpoints. The bandwidth of the HS, which presents a sequence of discrete apertures to the viewer, is reduced through a predetermined viewing scope by the HS viewing window. Each aperture yields information for a single 2D image of the scene. The viewer's left and right eyes observe different perspectives of the scene, as viewed from different directions, so the viewer perceives stereoscopic vision due to the binocular parallax. When the viewer moves from one image to the other, the motion parallax is observed at discrete steps. The viewer is able to verge on an object but accommodation occurs either at infinity or at a certain virtual observation plane, i.e. the HS does not provide the accommodation cue.

The HSs can be divided into HPO stereograms and full parallax stereograms in accordance with the exhibited parallax properties. The HPO stereograms are recorded by a cylindrical lens which focuses the laser light within a narrow vertical slit and preserves intact propagation in the vertical plane. The HS of this type are often called multiplex stereograms [25]. Horizontal orientation of human eyes allows to discard the vertical parallax and still to obtain adequate perception of the shape of the objects and their location in space. This makes HPO HSs an effective approach for imaging 3D objects. If perspective views are taken from slowly moving objects, the HPO stereogram can display this motion by linking it to the parallax recording. Animated HSs can be also produced by sacrificing the vertical parallax to encode the motion of the object [26].

In the first produced HPO HS [27] the distance between the plane of perspective images capture and the tracking camera should correspond to the distance between the projection screen and the hologram plane. To view a non-distorted image produced by such a HPO HS the viewer eyes should coincide with the elemental holograms. To alleviate this requirement a two-step recording process has been invented in which the recorded HS becomes a master for optical transfer by using a phase conjugated illumination source into a second HS which is recorded to allow a more convenient viewing distance. One can spare the two-step recording process by creating pre-distorted images in the computer from the directional information encoded in the perspective images; thus the so called Ultragram HPO stereogram was invented [28, 29]. A variety of different methods has been developed for composing a HS. However, independently of the method, the HS can be considered as an array of Fourier transformed perspective images of the scene. Thus, the HS exhibits only one phase term which is related to direction of propagation [30]. Following the description of diffractive properties of a HS given in [31], the perspective images are composed from pixels (picture elements) which send light with equal intensity in all directions. The stereograms encode directional information. They can be composed by direls (directional elements) which emit a spherical wave with a controllable amount of intensity in each direction or from hogels (holographic elements) in the case of HS which emit a set of plane waves with controllable intensity in different directions [32]. In order

http://dx.doi.org/10.5772/53412

to ensure an accommodation and to improve a smooth motion parallax presentation in HSs a wafel (wavefront element) is introduced in [31] that send a controllable intensity of light with a controllable wavefront curvature in each direction. The HS composed from wafels is called Panoramagram [31].

The modern digital holographic printers, based on the HS principle, ensure an automated one-step printing process to produce full-color full parallax output which is viewable under white light illumination. The main steps of the printing process include i) acquisition of the perspective images; ii) post-processing of the acquired images to form parallax-related images for distortion free reconstruction; iii) holographic recording of the elemental holograms. The principle of HS printing is schematically depicted in Figure 2 for the case of a full parallax hologram adopting the optical scheme of the holographic printer proposed in [12, 13]. The authors coined a name a multidot recording method for the proposed technique. The parallax-related image, composed from information taken from different perspectives, is displayed by means of a SLM. The SLM can be transparent or reflective liquid crystal display (LCD) [33] or digital micro-mirror device (DMD) [34]. Holographic recording corresponds to a Denisyuk type reflection hologram. The illuminating coherent light beam from a laser source is split into mutually coherent object and reference beams. The object beam illuminates the image displayed on the SLM. It is focused by a high numeric aperture lens on the exposed area of the hologram plate that comprises the elemental hologram. The other names have been introduced for the elemental holograms as hogels [32] or holopixels [35]. In this chapter we adopt the name hogel. The hologram plate is positioned close to the focal plane of the lens. To improve the illumination conditions on the hologram plate, a diffuser can be introduced in the object beam [6, 36, 37]. Exposure of the remaining part of the hologram is prevented by using a masking plate. The reference beam illuminates the exposed area from the opposite side to form a thick reflection hologram in the photo-sensitive layer of the plate. The light is reflected from the hologram in accordance with Bragg's diffraction which makes possible reconstruction under white light illumination. A full color HS can be recorded onto a panchromatic recording material with three lasers which emit at the wavelengths of the primary colors [38]. The lasers emit in a longitudinal mode and provide a beam with a TEM00 spatial structure. In some set-ups there is a masking plate with an aperture size equal to the hogel size between the light-sensitive layer and the reference beam. The hologram plate is sequentially translated in the horizontal and vertical planes with a X-Y stage until its whole surface is exposed. Thus both horizontal and vertical parallaxes can be recorded. Exposure time of each hogel and translation of the holographic plate are controlled by computer. The hogel encodes the directional information and intensity which comes from all points of the 3D scene to be imaged. This directional information varies with the location of the hogel in the hologram plane. When illuminated, the hogel creates an image of a small color patch with a given intensity for a certain viewing direction. The color patches reconstructed by all hogels in a given direction form one of the acquired perspective images. The reconstructed perspective image changes with the change in viewer's position. The acquisition and post-processing of the perspective images can be entirely separated in space and time from the holographic recording. The hogel encodes information from a large number of pixels which correspond to the number of perspective images.

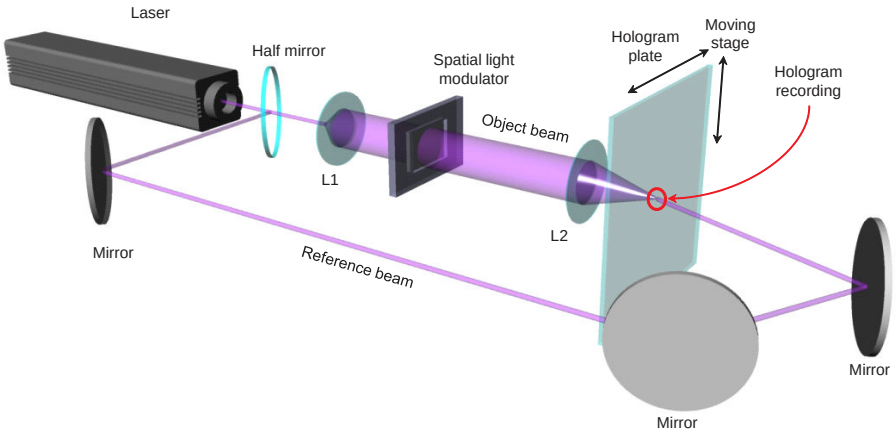

Figure 2. Schematic of the holographic stereogram printer.

Different improvements of this classical scheme for printing HSs have been proposed. The multidot printing method in [13] has been extended for printing HS of a rainbow hologram type and multicolor HS [39] as well as for 3D imaging by using a specially designed holographic screen and a transparency printed by a laser printer with a parallax information [40]. Taking in view the difficulty to obtain recording with a high diffraction efficiency in the Fourier plane of the lens due to the relatively narrow spectrum carried by the object beam, pseudo-random diffusers have been invented independently by [36, 41]. An ordinary ground glass diffuser spreads the light outside the hogel both in horizontal and vertical directions. This causes a light loss and hence entails increasing of exposure time. In addition, for HPO stereograms such a diffuser may worsen the image quality in vertical direction. A digitally designed pseudo-random band-limited diffuser in the object beam path improves uniformity of illumination of the hogel [41]. Two holographic diffusers, which can redirect up to 100% of the falling light, are proposed in [37] to be used with HPO stereograms. The first one is manufactured by recording a hologram of the strip diffuser. The second type is produced by recording a HPO stereogram of a rectangular point diffuser. The holographic diffuser is mounted in a close contact with the SLM to project the real image of the diffuser on the hogel. In the second case a multiple-point holographic diffuser is reconstructed. In [14] a special lens is introduced in the path of the object beam close to the holographic plate to control the HS resolution. The same authors also proposed to replace the masking plate by a specially designed holographic optical element which acts as a variable band-limiting diffuser that redirects the object beam to uniformly illuminate only the area of the hogel. The latter together with a changeable reference beam masking plate allows to record hogels of variable size. The proposed printer can be also used for production of animated stereograms. A special system of an aperture and a 2D microlens array is used in Geola printers [35] to form hogels or holopixels of variable size and shape. HS technology is applied in Zebra Imaging [42] in USA using DuPont photopolymers, 3D Holoprint [43] in France using Ultimate' silver halide

http://dx.doi.org/10.5772/53412

materials, Inline holography Inc. in Canada and others. A holographic printer which produces an animated HS in vertical direction with preserving the full parallax information in the horizontal direction is proposed and tested in [44]. The animation effect is observed by scrolling the hologram in vertical direction. The holographic printers developed and patented by Geola [15,16] are fully described in [18,35]. The color HSs can be recorded by using a multiple exposure method [45] or primary color mosaic method. In the first method the beams from the RGB lasers are combined to form a single beam and expose simultaneously each hogel. The quality of the recording depends on the dynamic range of the photo-sensitive material [38]. The main disadvantage of this method is the cross-talk between the separate color channels [46]. In the second method a space division of exposures for the primary colors is applied which, however, decreases three times the diffracted intensity. A method of color management for a full-color holographic 3D printer for HSs under RGB lasers illumination is proposed in [47] through the spectral measurement of the reconstructed light. Different hogel sizes have been reported from 0.4 mm × 0.4 mm up to > 2 mm × 2 mm in [18] and 0.2 mm × 0.2 mm in [47]. Decrease of the hogel size to make it comparable to the pixel size of the digital displays entails rise in printing time. To speed the recording process more powerful CW lasers and SLMs with higher refreshing rate should be used. Pulsed lasers are more suitable for this task from the point of view of stability of the printing system. Parallel exposure of several hogels is tested in [48].

2.2. Acquisition and post-processing of perspective images

Acquisition of the perspective images needs a tracking camera or modeling by a computer using different rendering methods. It is also possible to combine captured images with digitally rendered. The images are further processed to be recorded as hogels. At proper acquisition of the perspective images the HS can provide the viewer with an animated image. Image acquisition for the case of a HPO is shown in Figure 3(a), where the camera takes images along the horizontal axis only, and no acquisition is made along the vertical axis. The main advantage is a strongly alleviated requirement for the number of the required 2D images at the expense of viewer's eyes location only in the horizontal plane. The capture procedure for a full parallax HS is shown in Figure 3(b), where the camera takes images along both horizontal and vertical axes. The number of the acquired images is squared which is the most essential drawback of this approach. The nowadays HSs, printed by the modern holographic printers, can boast with size up to 1 m × 1.5 m and field of view (FOV) about 100 degrees [18]. The recent advances in laser technique, computers and SLMs make possible fabrication of HSs with a very high spatial resolution. This entails capture or modeling of thousands of perspective images. For real-life scenes these images should be acquired for a short time on the order of a few seconds.

In the dawn of the holographic printing, the systems for capture of perspective images comprised a camera facing an object which was placed on a rotating stage [7]. Such a system introduced a keystone distortion in the captured images, but this distortion was considered as a minor drawback because of the low quality of the printing itself. Later, two methods for acquisition of perspective images were developed as the simple camera method and the recentering camera method [27]. The simple camera method provides the simplest geometry

for acquisition and rendering due to the invariable FOV of the camera during the capture process, as is shown in Figure 4. The forward facing camera, preferably with a large FOV, captures perspective images, while being translated equidistantly along the horizontal (or vertical) axis. The leftmost camera C_{LM} and rightmost camera C_{RM} take images, which are shown in Figure 5. The acquired images give different perspective representation of the object. The shortcoming of the simple camera method is that the object in the images is surrounded by a large non-informative area, and the number of pixels used for object representation is reduced leading to possible decrease of resolution too. Thus, the simplicity of rendering of the simple camera method is counter-balanced by worsened resolution and unavoidable non-informative area in the images. In addition, the camera with a large CCD is required and the lens of the camera should obligatory have a large FOV which may introduce severe distortions in the captured images.

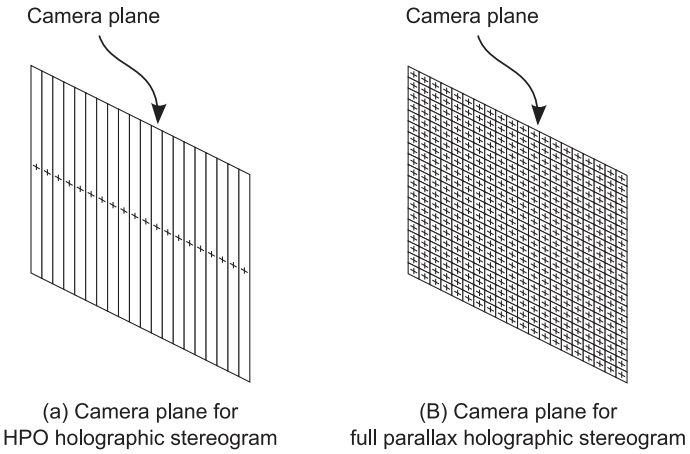

Figure 3. Acquisition of perspective images for a holographic stereogram.

The main drawback of the simple camera method is removed by a recentering camera method, whose acquisition geometry is shown in Figure 6. It is similar to the simple camera capture of the perspective images along the horizontal axis at equidistant intervals, but in this case the camera is provided with a recentering camera configuration to position the acquired objects in the center of the images. The acquired images by the recentering camera in the leftmost and rightmost positions in Figure 6 are presented in Figure 7(a) and (b). The non-informative area is reduced. Although implementation of this approach is more complicated, it enables taking higher resolution images. The figures depict translation only along the horizontal axis; generalization to translation in the vertical plane is straightforward. The recentering camera method is a good model to be used for computer generation of the perspective images. However, for capture of real-time scenes this method requires sophisticated expensive equipment and puts severe demands on the speed of the movement of the CCD array inside the camera. The required lens with a large FOV may also distort the captured images.

http://dx.doi.org/10.5772/53412

An effective solution for improvement of image acquisition while keeping the advantage of a simple camera method rendering has been recently proposed [49]. In the proposed solution the camera with an ordinary FOV rotates while being translated. The captured image is undistorted in a vertical plane which is normal to the central ray passing through the camera, but it is distorted in a plane parallel to the hologram plane. That's why the proposed image capture is a two-stage process. The sequence of the captured images is further preprocessed to transform them into images corresponding to a virtual forward-facing non-rotatable camera with a substantially wider FOV as if it is translating along a rail. The second sequence of images is used to compose the HS. The transformation procedure and the interpolation algorithm developed to decrease the noise which may be introduced by the pixel swapping transformations are thoroughly patented [49].

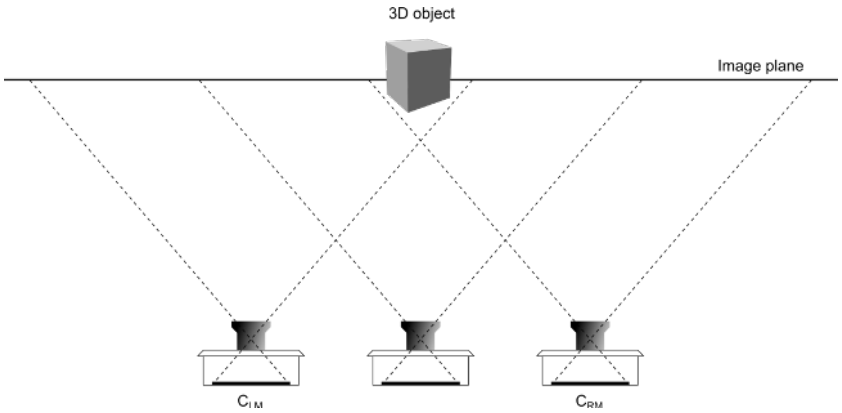

Figure 4. Simple camera method.

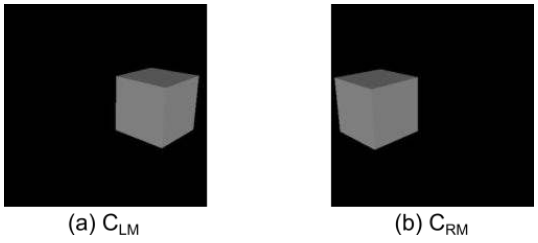

Figure 5. Image capture by the simple camera method.

To view distortion-free reconstruction comparatively far from the hologram [27], perspective images should be rearranged to form the separate parallax or "hogel" images corresponding to different hogels in the hologram plane, as it is shown in Figure 8. Both perspective and hogel images are 2D arrays with, in general, different dimensions. The perspective images

P_{kl}, $k=1..n$, $l=1..m$, compose a stack Φ of $n \times m$ images, where n and m are the number of images captured in horizontal and vertical directions, and k and l are indices which give the camera position at image capture in 1D or 2D grid in Figure 3. Each perspective image consists of $N \times M$ pixels. The size of the hogel images is $n \times m$ whereas their number is given by $N \times M$. The pixels in the hogel images are arranged in the order of capture of perspective images along horizontal and vertical axes. The hogel image h_{ij} is composed from (i,j)-th pixels in all perspective images in Φ as follows:

$$h_{ij}(k,l) = P_{kl}(i,j), k = 1..n, l = 1..m; i = 1..N, j = 1..M \tag{1}$$

The hogel image h_{ij} is displayed on a SLM and recorded in a focal plane of a lens as an elemental hologram by means of a reference beam in the (i,j)-th hogel in the hologram.

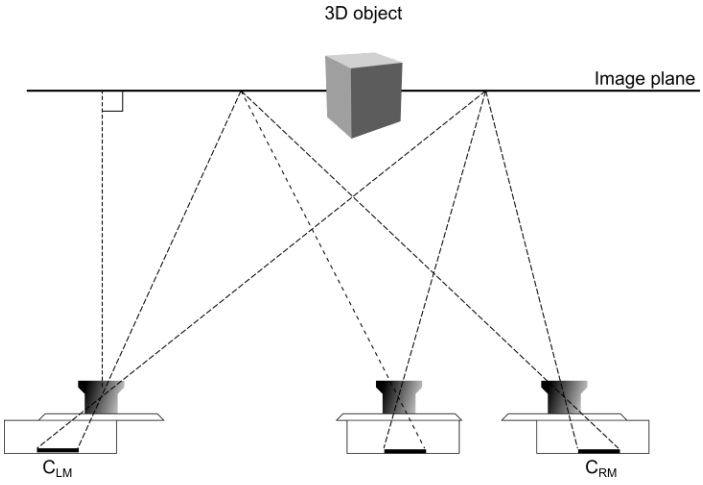

Figure 6. Recentering camera method.

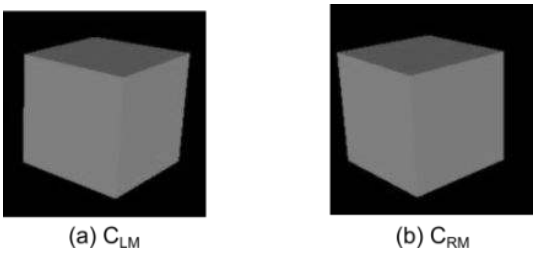

Figure 7. Image capture with the recentering camera.

http://dx.doi.org/10.5772/53412

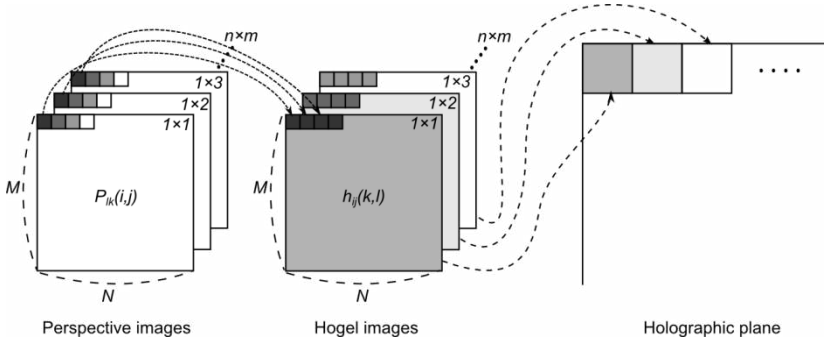

Figure 8. Rearrangement of perspective images into hogel images.

2.3. Distortions deteriorating the reconstructed image

The light modulated by the hogel image displayed on the SLM passes through optical components, such as objective or telecentric lenses, which may cause radial distortion [50]. As shown in Figure 9, the radial distortion can be categorized by two ways - a pincushion distortion and a barrel distortion. In the case of an "ideal" optical system the hogel image is recorded without any distortion, and it shows uniform angular intensity distribution within a FOV. When the hogel image is recorded with pincushion distortion, the angular intensity distribution is dense at the center and sparse at the edges of the viewing zone, and vice versa in the case of barrel distortion. Figure 10 depicts angular distributions corresponding to different distortions. The distortions cause changes in direction and range of the angular intensity distribution of the hogel image, which means the observer will see a distorted image. Figure 11 shows the shifted position of the observer by radial distortion. The radial distortion is given by

$$X_u = X_d\left(1 + k r_d^2\right), \quad Y_u = Y_d\left(1 + k r_d^2\right), \quad r_d = \sqrt{X_d^2 + Y_d^2} \tag{2}$$

where X_u and Y_u give the original position of the pixel, X_d and Y_d correspond to the shifted position of the pixel due to the radial distortion, r_d is the radius of the radial distortion, and k is a distortion coefficient.

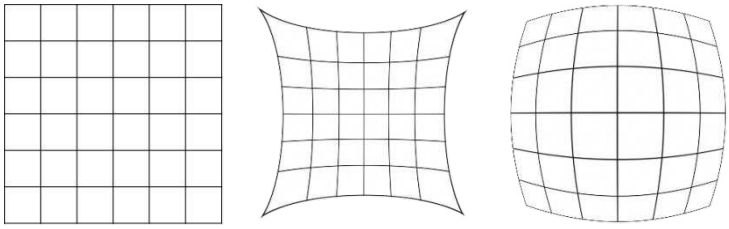

Figure 9. Examples of radial distortion: (a) none distortion, (b) pincushion distortion, (c) barrel distortion.

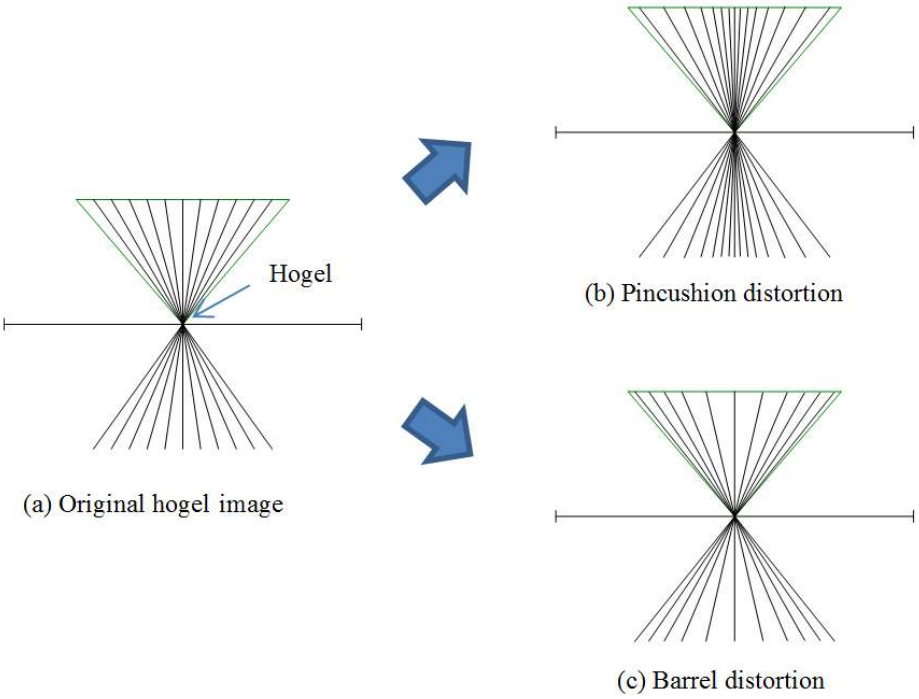

Figure 10. Angular distributions of rays at different radial distortions.

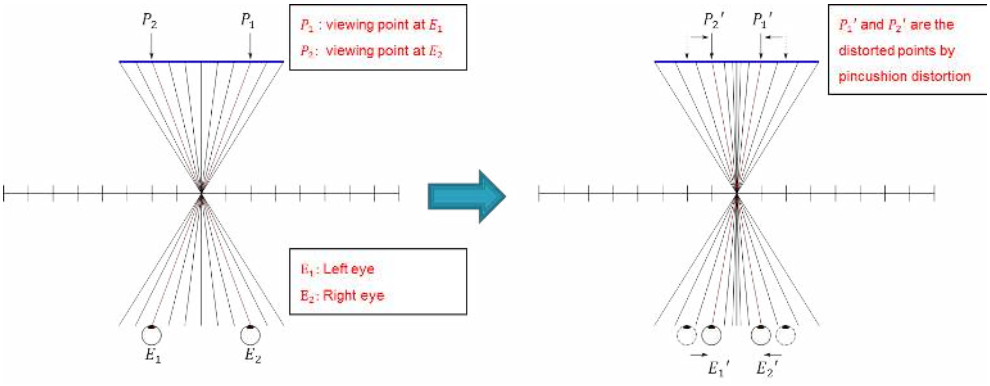

Figure 11. Movement of viewing point by pincushion distortion.

The pixelated structure of the HS and the way of building the reconstructed 3D image make them discrete imaging systems which can exhibit aliasing artifacts. The HS is characterized with an angular sampling and spatial sampling of the reconstructed image. Both sampling

http://dx.doi.org/10.5772/53412

rates are related. Angular spectrum depends on the spectrum of the object to be imaged and is determined by the SLM parameters. In the holographic plane the sampling is given by the size of the hogel. The view-based analysis which is usually applied to HSs is an effective tool to predict forming of the 3D images but it is not always capable to explain their distortions. The study of these distortions needs to apply both wavefront analysis and sampling theory [24,27]. The wavefront analysis is based on the incoherent imaging. Analysis of image artifacts of HPO HSs based on imaging of a single point which creates a spherical wavefront is made in [24]. To the contrast with a hologram, the HS creates piecewise approximations to the wavefronts of the spherical waves emitted by the object's points. If the size of the hogel is too large the piecewise approximation is undersampled which results in visual artifacts as e.g. jumping of the reconstructed image when the viewer is moving along the HS. Quantization of the wavefront introduces phase errors. They are due to the fact that a wavefront from a point with an arbitrary depth is reconstructed as a wavefront of a point localized in the image plane of the HS. For a point which is located in front of the image plane of the HS the segmented wavefront has a less curvature than the real one and vice versa for a point behind the image plane. In [51,52] an expression for the optical transfer function of the HPO HS is derived which relates together the size of the hogels, the depth of the imaged scene and the resolution of the reconstructed image. The modulation transfer function falls rapidly with the spatial frequency for hogel sizes below 1 mm [52] which shows that some optimum size should be found to preserve the good quality of the reconstructed images. The optimum hogel size depends on the requirements of the human visual system, viewing distance, object depth and proper sampling of perspectives in the viewing angle. The hogel size should ensure smooth perception of the motion parallax and smooth spatial reconstruction of images. These are to a certain degree contradictory requirements. The decrease of the hogel size inevitably leads to lower number of reproduced directions due to the diffraction limit. Measurement of the angular resolution of diffracted light for a full-color HS was undertaken in [53] with sizes of the elemental hologram varying from 50μ m× 50 μm up to 400μ m × 400 μm. It is shown that the size 50μ m× 50 μm provides angular resolution of 1.08 deg., which can satisfy the angular resolution required by the human visual system.

2.4. Simulation of reconstruction of full-parallax holographic stereograms

Despite the progress made in the recent years, the holographic printing of large format digital holograms is expensive and in most of the cases time consuming undertaking. Separated by location and time capture and holographic recording require replaying of the composed HS by computer. In other words, to have freedom during the design process one should be able to check the quality of reconstruction from the designed HS by simulation before it is fed to the actual physical device. This makes development of appropriate simulation tools a pressing task. Software for obtaining a preview for a HPO HS produced from a web camera video stream is reported in [54].

The viewer perceives intensity provided by all printed hogels within the angular intensity distribution related to the particular viewer location. Each hogel encodes angular distribution of intensity corresponding to a certain small part of the visualized 3D object or scene when

this part is viewed from multiple angles. The inputs from different hogels come from different pixels of the corresponding hogel images, as is depicted in Figure 12. For convenience, we derive the simulation algorithm for a single horizontal line of the hologram which is oriented along the X axis. Derivation of the algorithm for the whole hologram is straightforward. We assume that the viewing point $E(x, z)$ is located at a certain observation distance, D, from the hologram plane (Figure 12a). The Z axis points to a virtual observation plane (image plane) which is parallel to the hologram and contains the overlapping inputs from all hogels. The virtual observation plane is also located at distance D from the hologram plane. Let us consider the input to the viewer from a given hogel on the hologram plane. The size of the hogel is so small in comparison to the distance D that we can consider it as a point which creates angular distribution of intensities in the virtual observation plane, as it is shown in Figure 12b. The input from the hogel is determined by the angle, θ, corresponding to the line which passes through the viewer location and the hogel. We choose the hogel position as an origin of the (X, Z) coordinate system. From the point E (x,z) the viewer gets the intensity from the point P in the cross-section of the virtual observation plane with the angular spread of intensities provided by the hogel. The value of this intensity is found from the hogel image pixel which encodes the direction given by θ. We introduce an auxiliary axis ξ in the observation plane that is parallel to the X-axis. The width of the patch in the observation plane with intensity input from this hogel is calculated by

$$W = 2D\tan\left(\frac{\phi}{2}\right) \tag{3}$$

where φ is the angle which gives the spread of the angular intensity distribution attached to the hogel. The sampling step, Δξ, of the intensity values distribution in the observation plane is given by $\Delta\xi = W/n$, where n is the number of samples of the intensity distribution encoded in the hogel along a single row. The index of the pixel, n_P, which encodes the intensity at point P is determined by

$$n_P = \mathrm{I}\left\{\frac{W/2 + \xi_P}{\Delta\xi}\right\} \tag{4}$$

where ξ_P is the coordinate of P, and $I\{\}$ is an operator which takes the closest integer value of the expression in the brackets. Since the sampling step, Δξ, is constant in the virtual observation plane, the uncertainty in estimation of direction of the hogel input varies along the auxiliary axis, ξ. It is maximum at the center of the hogel at $x = 0$, where it is approximately equal to $2\tan(\phi/2)/n$ radians, and decreases to its ends becoming $\approx 2\sin(\phi/2)/n$. Actually, $|\xi_P|$ is the distance from the point at which the normal from $E(x, z)$ to the hologram intersects its plane. Thus, for an arbitrary viewer location one easily calculates the resulting intensity of rays coming from all hogels at a given point of the virtual observation plane, which makes the numerical reconstruction of the HS for any location of the viewer feasible.

http://dx.doi.org/10.5772/53412

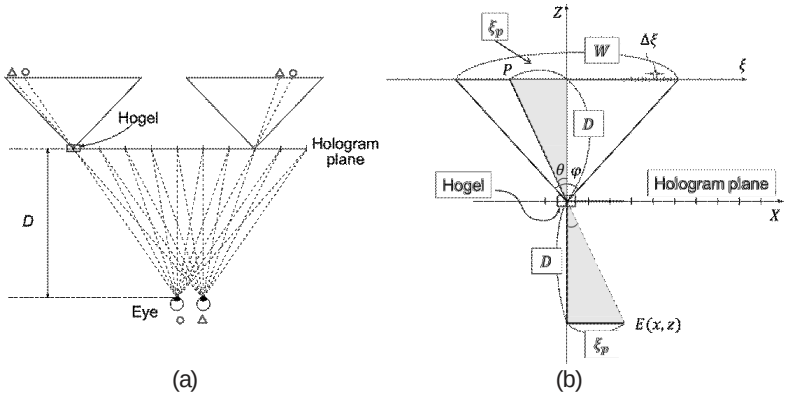

Figure 12. a) Geometric relation between the viewer and the hologram plane, (b) intensity input from a hogel to the viewer's location.

Figure 13. a) Perspective images from different views, (b) example of a hogel image.

To check the developed approach, we made simulation of all steps involved in the synthesis of a HS with its further numerical reconstruction. We assumed that hologram plane was composed from 100× 100 hogels and each hogel image consisted of 100× 100 pixels, which means that capture of 10,000 perspective images of a 3D object was simulated by using computer. In this test, we used a computer simulated 3D scene. The perspective images were rearranged to form 10,000 hogel images. The perspective images were captured by the recentering camera method, and some of them are shown in Figure 13(a). For illustration, examples of the composed hogel images are presented in Figure 13(b). The generated 10,000 hogel images were used as an input data for numerical reconstructions of the holographic stereogram which was supposed to be recorded. The numerical reconstructions for some arbitrary viewer's locations along the horizontal and vertical directions are shown in Figure 14. The good quality of reconstruction from the synthesized stereogram is obvious.

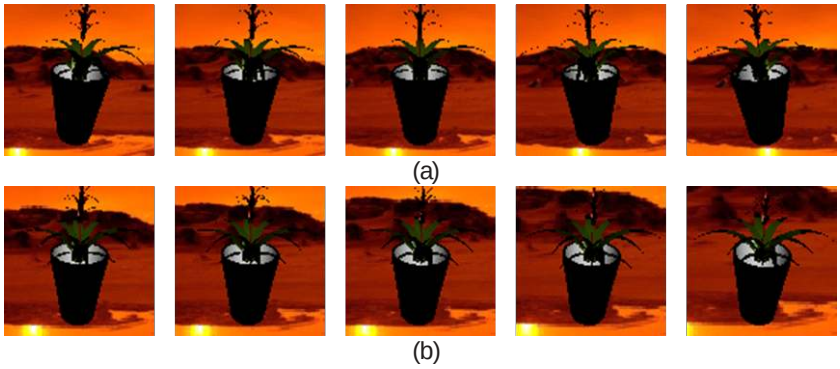

Figure 14. a) Numerical reconstruction results at 500 mm (angle interval 10 degree), (b) numerical reconstruction results at fixed *X* and *Y* coordinates.

2.5. Hardware issues and light-sensitive materials

To illustrate in practice printing of HSs we give the description of the developed by us holographic printer (Figure 15). The specifications of the main system's components are given in Table 1. The beam from a laser emitting at 532 nm is divided by the first polarizing beam splitter (PBS) into two optical paths, and the intensity ratio of two beams can be adjusted by a half-wave plate. The laser beam which passes through the PBS1 is the reference beam, whereas the other one reflected by the PBS1 is the object beam. The object beam is expanded by two lenses, L1 and L2, and illuminates the amplitude type SLM by using the PBS2. The beam is spatially modulated by the hogel image which is fed to the SLM as a bmp file. The modulated beam is focused onto the holographic emulsion by the lens, L3. The reference beam is also expanded by two lenses L4 and L5, in order to provide a beam width, which covers the hogel in the hologram. The reference beam impinges the holographic plate at 45 degrees. The interference pattern produced by the object beam and the reference beam in the holographic emulsion is recorded as a volume hologram. The holographic plate is moved by a X-Y stage along horizontal and vertical axes at a given spatial step, which coincides with the hogel size. Through such a procedure, each hogel is recorded at the desired hogel position. The shutter controls the exposure time of the hologram which is a product of the material's sensitivity and the laser power. The accuracy of the shutter is crucial. The time sequence of shutter operation is shown in Figure 16. The shutter goes into an open state after the shift of the X-Y stage, the time, required for the system to settle and for loading the hogel image on the SLM. The X-Y stage coordinates the shift of the optical header. The moving precision of the device is about 1 μm. Typically the stage can be driven by two types of motors: i) a step motor which is cheap and easy to handle but with a lower precision; ii) a linear motor which is more complicated and expensive but with higher precision. We use a step motor in our set-up. Due to the advances in modern computers and software a personal computer can be used as a holographic printer controller. However, it is still recommendable to use a microprocessor for a high-speed and real-time system.

http://dx.doi.org/10.5772/53412

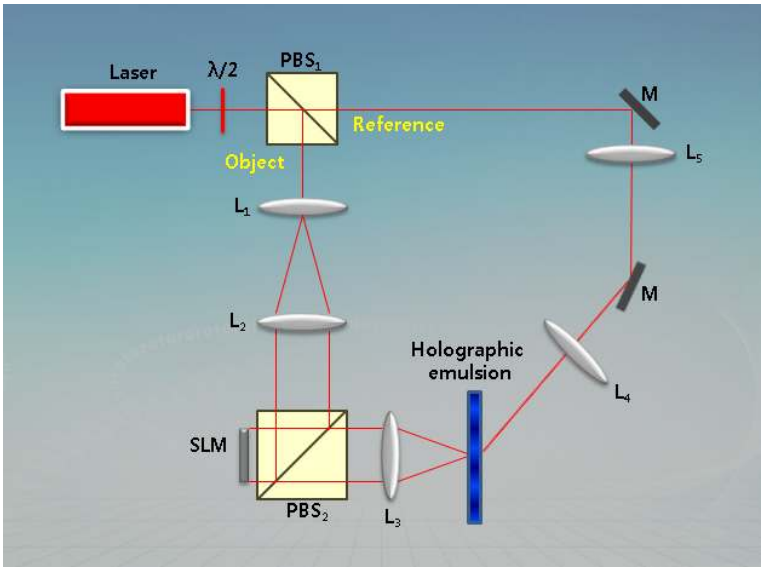

Figure 15. Schematic of the holographic printer.

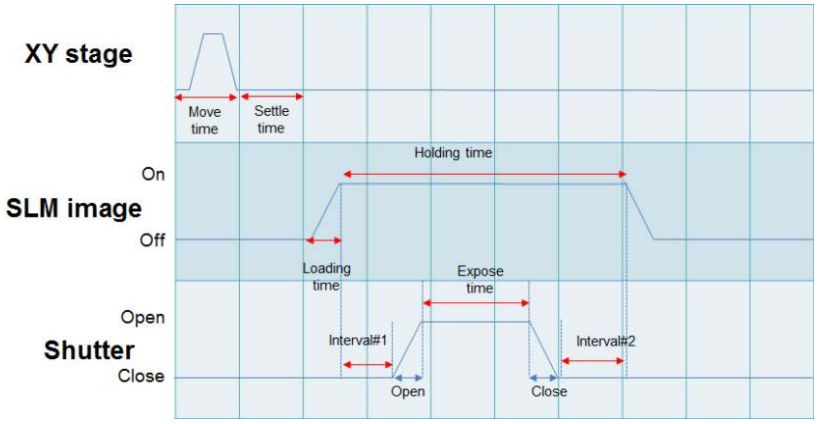

Figure 16. Time sequence of shutter operation.

Production of stable reproducible hard-copies by a holographic printing, based on recording of volume holograms, requires reliable medium for permanent multicolor (RGB) holographic recording with high diffraction efficiency, sensitivity, resolution and signal-to-noise ratio across the visible region. The dichromate gelatin, photopolymers and silver halide provide parameters close to the requirements [55]. The non-satisfactory spectral response and low sensitivity of the dichromate gelatin exclude it from the list of candidates despite its low losses

and high diffraction efficiency. The photopolymers, in which the phase modulation is formed due to photoinduced changes, allow simple rapid processing and practically 100% diffraction efficiency, but they still exhibit comparatively low sensitivity, resolution and dynamic range. The silver halide emulsions are discrete carriers media in which recording occurs in nano-sized particles dispersed in a carrying gelatin matrix. They can boast with high sensitivity in a broad spectral range, diffraction efficiency of 80-98%, high resolution and dynamic range as well as long-term storage [55]. The drawback of the silver-halide emulsions is the low signal to noise ratio in the blue spectral region due to the light scattering. Recording of volume reflection holograms needs resolution > 6000 mm^{-1} which is realized only with ultra-fine-grain silver halide materials. The materials PFG-03C produced by the firm Slavich, Russia [35, 56] has about 12 nm size of initial silver halide crystals and exhibit low signal-to-noise ratio in the blue spectral region. The scattering in this region is decreased by nanosized emulsions with the average grain size about 8 nm. Such quality is provided in Ultimate holographic plates [57] or in the plates HP-P [55], Bulgaria.

SLM	**Type**	**Amplitude type (liquid crystal on silicon)**
Number of pixels	1920 × 1080 pixels	
Pixel interval	7 μm	
Laser	Power	100 mW
	Wavelength	532 nm
Holographic emulsion	Emulsion	ULTIMATE-08
	Grain size	8 nm

Table 1. Specifications of the holographic printer

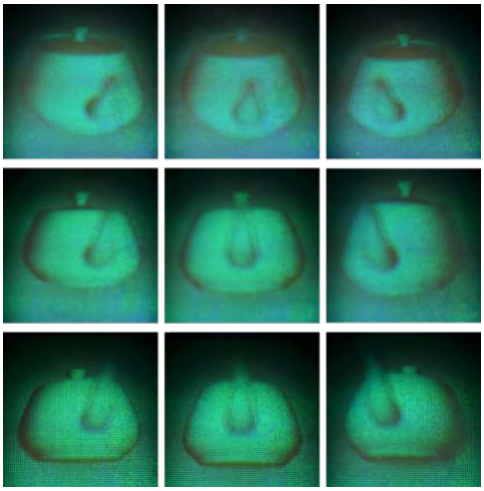

Figure 17. Optical reconstruction from a printed holographic stereogram along the horizontal and vertical directions.

http://dx.doi.org/10.5772/53412

We used in our printer system the Ultimate 08 emulsion with exposure 200 μJ/cm^2. We summarized the specifications of this emulsion in Table 2 [57]. The typical exposure time of this emulsion for He-Ne laser varies from 4-5 s at 5 mW power and 6.1 cm × 6.1 cm size of the holographic plate to 30-40 s at 25 mW for a 30 cm × 40 cm plate. Developing time is about 6 minutes at 20 C° - 25°C, and a bleaching agent is also used. The calculated hogel images were expanded 10 times before being applied to the SLM. Thus, a matrix of hogels is formed in a hologram plane. Figure 17 presents the photos taken from different locations of the image reconstructed at white light illumination from the HS of a computer graphic model of a teapot.

Emulsion	Application	Sensitivity (uJ/cm^2)	Grain size (nm)/ Resolution (lines/mm)	Lasers	Lifetime (at 4°C)
Ultimate 08-mono-chrome	For transmission and reflection holograms	150-200	8/10000	Continuous and pulsed: all colors	> 2 years
Ultimate 08-color	For reflection holograms (RGB)	120-150/ color	8/10000	Continuous : R+G +B	> 2 years
Ultimate 15	For transmission and reflection holograms (RG)	75-100	15/7000	Continuous and pulsed : R+G	> 1 year
Ultimate 25	For transmission holograms (pulsed lasers), Brighter and much less noise, U25 needs more energy.	10-30	25/5000	Pulsed lasers: Ruby, YAG	> 2 years

Table 2. Ultimate hologram emulsion specification

3. Printing of holographic fringes

The white viewable HSs spatially multiplex 2D images and hence do not reconstruct a real 3D image. Computer-generated holograms (CGHs) based on modeling of a holographic interference pattern create a true 3D impact [58]. That's why a lot of efforts have been dedicated to printing of CGHs whose calculation is based on rigorous diffraction. Two problems must be overcome when solving this task – the time-consuming calculation of the fringe pattern and the requirement for high spatial resolution of the printer in order to ensure a large viewing angle. Increase in resolution entails rise in the computation time.

3.1. Methods for computer generation of holographic fringe patterns

A fast holographic fringe pattern generation algorithm is required for the wavefront printing. The Rayleigh-Sommerfeld (R-S) integral gives an exact fringe pattern corresponding to a

desired object. The object is represented as a set of self-emitting points giving a light field with a complex amplitude which at the point (x, y) in the plane of the hologram is the sum of the spherical waves coming from all points of the object:

$$O(\xi, \eta)=\sum_{p=1}^{N} \frac{a_p}{r_p}\exp\left[j(kr_p+\varphi_p)\right], \quad r_p=\sqrt{(\xi-x_p)^2+(\eta-y_p)^2+z_p^2} \tag{5}$$

where (x_p, y_p, z_p) are the Cartesian coordinates of the object's point, a_p and φ_p are the amplitude and the phase of the light field emanated by this point, and r_p is the distance between this point and the point on the hologram; $k=2\pi/\lambda$ is a wave number, λ is the wavelength. Since in the equation of the hologram intensity, $H=|O+R|^2$, where $R(\xi, \eta)=a_r\exp(j\varphi_r)$ is the reference wave with an amplitude a_r and phase φ_r, the only relevant term is $H=2Re\{OR^*\}$, the so called bipolar intensity approach has been invented [32] that allows to calculate the fringe pattern

$$H_{bi}(\xi, \eta)=\sum_{p=1}^{N} \frac{a_p}{r_p}\cos(kr_p+\varphi_p+\varphi_r), \tag{6}$$

by using only the real numbers where we assume that $a_r=1$. However, one of the substantial drawbacks of the R-S method is its quite high computational complexity. To overcome this bottleneck, different fast algorithms for implementation of (6) have been developed for flat holograms and more sophisticated geometries as a cylindrical or a disk hologram which provide an increased viewable area [59,60]. The fast algorithms for computer generation of cylindrical ordinary and rainbow holograms [61, 62], for generation of a master disk hologram [63] and image plane hologram [64] have been reported. Although these holograms are based on the same underlying optical principal, the associated computer generation algorithms undergo different modifications according to the characteristics of each hologram. A successful approach, especially for holographic printing, is the partitioning based algorithm for computer hologram generation. The hologram plane is divided into $M \times N$ multiple segments with $m \times n$ elements each, and a set of approximations to calculate the distance in (5) is applied to each segment. For example, the distance between the object and the hologram in the case of a cylindrical hologram is practically fixed and not large enough to use the Fresnel approximation. In this case the distance, r_p, is computed by means of two look-up tables which are composed for each segment in such a way as to give the distance between the object point and the point located along the vertical and horizontal central lines in the segment. To decrease the spatial frequency in the plane of the hologram, the computation is performed with a spherical reference wave in a Fourier lenless geometry when the reference point source is positioned close to the object and at the same distance from the hologram [61]. The same approach with two look-up tables has been applied for generation of the disk hologram [63]. For a rainbow hologram the computation is made for 1D hololine. Calculation of the image-plane hologram requires introduction of a small positive value in the denominator in (6) to avoid the high divergence of fringes for object points which are too close to the hologram plane [64,65]. In this case the sign of the phase of the object beam depends on which side of the hologram is the object's point. 360 degrees viewable hologram requires removal of hidden

http://dx.doi.org/10.5772/53412

surfaces to ensure proper reconstruction of the object [66]. This problem is solved by forming the correct object data for generation of the hologram for different viewpoints. For the purpose, perspective images from different viewpoints are taken. The acquired intensity distributions are combined with the depth information provided by a computer graphics model to yield 3D coordinates, amplitudes and phases corresponding to all point sources that constitute the object.

There have been developed a series of algorithms such as phase-added stereogram (PAS) [30, 67], compensated phase-added stereogram (CPAS) [68, 69], accurate phase-added stereogram (APAS) [70], and accurate compensated phase-added stereogram (ACPAS) [71]. Although the ACPAS gives a better quality, still it has some unwanted noise which is due to the inaccurate numerical model. As an improved version, we propose a novel digital hologram generation algorithm which we call fast phase-added stereogram (FPAS). The numerical model of the FPAS is expressed as,

$$H_{FPAS}(\xi, \eta) = F^{-1}\{I(\upsilon, \nu)\}, \tag{7}$$

$$I(\upsilon, \nu) = \sum_{p=1}^{N} \frac{a_p}{r_p} \exp\left(jkr_p + \varphi_p\right) \exp\left\{j2\pi[\upsilon_p(\xi - x_p) + \nu_p(\eta - y_p)]\right\}, \tag{8}$$

where, $H(\xi, \eta)$is the holographic fringe pattern, $I(\upsilon, \nu)$is the spatial frequency distribution in the spatial frequency domain, p is the index of points, $N$is the number of points, $r_p$is given by (6), a_p is complex amplitude of the p-th point, $\exp\left(jkr_p\right)$ is the phase, and last term in the sum is a complex sinusoidal function. The spatial frequencies u_p and ν_p are determined as

$$\upsilon_p = \frac{\sin\theta_{\xi p} - \sin\theta_{\xi \mathrm{ref}}}{\lambda}, \qquad \nu_p = \frac{\sin\theta_{\eta p} - \sin\theta_{\eta \mathrm{ref}}}{\lambda}, \tag{9}$$

where, $\theta_{\xi p}$and $\theta_{\eta p}$ are the incident angles from the associated object point, and $\theta_{\xi \mathrm{ref}}$ and $\theta_{\eta \mathrm{ref}}$ are the illuminating angles of the reference wave forξ and ηaxes.

The geometry of the coherent stereogram calculation is shown in Figure 18. In the first step the hologram plane is partitioned into suitable square shape segments. The fringe pattern over each segment is approximated as a superposition of 2D complex sinusoids, where each such sinusoid approximates the contribution of each object point to the hologram pattern over one segment. Therefore, a spectrum associated with each segment is easily constructed by placing the amplitudes of complex sinusoids to correspond to frequency locations. The spatial frequencies associated with the contributions of points in a point cloud are quantized to a discrete domain by moving them to their nearest allowed discrete frequency value without changing their complex amplitudes. This modification is an additional source of distortion in the reconstruction. In the second step, the spectrum of a segment, that is composed of complex amplitudes of 2D complex sinusoids, is transformed by IFFT to convert the spectrum to the associated fringe pattern. This procedure is repeated for each segment to complete the computation. An arbitrary hologram function over one segment, representing the spatial

coordinates in a plane, can be written as a superposition of harmonic functions. Each harmonic function is the inverse Fourier transform of a single impulse function which corresponds to a single object point with a complex amplitude. Due to the linearity of the Fourier transform, the IFFT of the spectrum of a segment, which is composed of contributions from all 3D object points, yields the hologram over that segment.

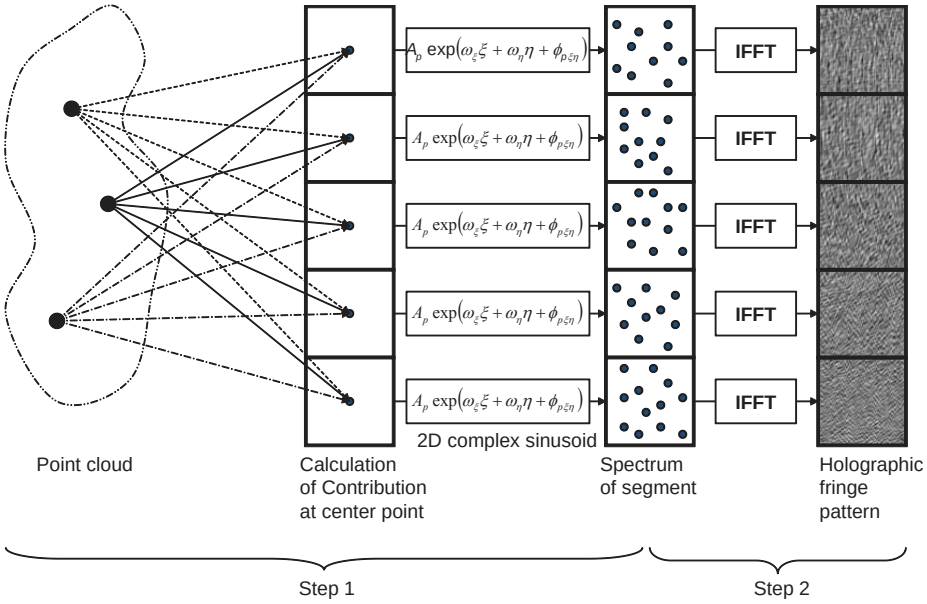

Figure 18. Geometry of fast phase-added stereogram calculation.

Three holographic fringe patterns generated by using R-S integral, ACPAS and FPAS algorithms corresponding to a single self-illuminating object are shown in Figure 19. For the ACPAS and the FPAS, the used segmentation size and FFT size are 4 × 4 pixels and 8 × 8 pixels, respectively. As shown in Figure 19, the R-S integral gives exact fringe pattern, and even at the initial phase difference about 68 degrees between Figure 19(a) and 19(c), the fringe pattern from the FPAS algorithm is comparable to the R-S fringe pattern. However Figure 19(b) which is generated by using ACPAS algorithm looks worse when compared to the fringe patterns obtained by the R-S integral and the FPAS algorithm. This means that fine phase matching cannot be done by the ACPAS algorithm. Contrary to the ACPAS, the numerical model of the FPAS is acceptable, and fine phase matching can be done by the exact phase distribution determination.

http://dx.doi.org/10.5772/53412

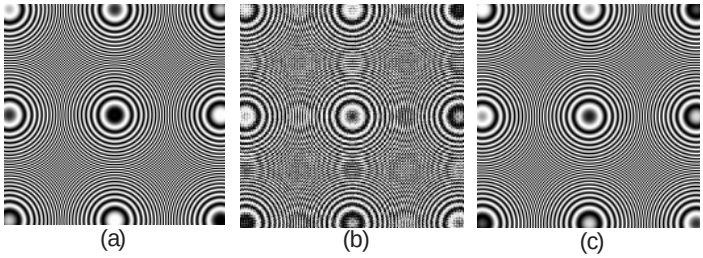

Figure 19. Generated holographic fringe patterns corresponding to a single self-illuminating object; (a) Rayleigh-Sommerfeld integral, (b) ACPAS, (c) FPAS.

3.2. Direct printing of fringes

Micro-processing techniques as e-beam writing or lithography, which provide excellent resolution and can be used for printing of holographic fringes, are too expensive for everyday use. This inspired development of low-cost fringe printers. Using of a laser printer for recording of a CGH is proposed in [72]. Printing of a CGH by using optical disk writing equipment is described in [73]. Printing of the fringe pattern by using a CD-R writer is proposed in [74, 75]. The printed hologram is reconstructed with a white light. Printing of the fringe pattern dot by dot of 3 μm in a diameter by scanning a laser spot on a holographic plate is reported in [76]. To increase the speed of printing the holographic film is placed on a rolling drum. A direct fringe printer in which a small part of the fringe pattern is displayed on a SLM and its demagnified version is recorded as a thin hologram is proposed in [21,22]. The demagnification on the order of 1/12 or 1/16 is achieved with a telecentric system of lenses. The SLM is illuminated with a laser light. In [62] a Nd:YAG+LBO DPSS laser emitting at 473 nm with power 5 mW is used. After the exposure the hologram is shifted with a highly accurate X-Y stage with a stepping motor. Precision of the X-Y stage is 4 μm. Resolution of the printed fringe pattern depends on the quality of optics used to transfer the image from the SLM onto the holographic film. A fringe pitch of 0.44 μm has been reported. The fringe printer was used for printing of a laser reconstructed cylindrical hologram with radius of 69.5 mm and pixel pitch 0.867 μm [61]. The produced CGH required 45 h computation time. The printer was used also for production of a computer generated master 360 degrees viewable portable disk hologram which was used for optical recording of a reflection hologram viewable with white light [63]. Recently, image-plane full-parallax hologram has been printed [64]. Fringe printing of an animated computer-generated cylindrical hologram which is calculated to show animation in horizontal direction is reported in [77].

3.3. Holographic recording of the wave-front diffracted from the fringes

The direct fringe printer records partitioned digital holographic fringe patterns into a holographic emulsion repeatedly in order to make a large SLM. Although the holographic fringe pattern is recorded into a holographic emulsion, it can be regarded as a thin hologram because it does not record the interference pattern with a reference wave. Due to such reasons, it should

be reconstructed under laser illumination. A volume hologram printer is proposed in [78] which records an interference pattern with a reference wave of the optical reconstruction from the holographic fringe pattern displayed over an electrically addressed SLM. This method provides several advantages such as fine wavelength selectivity for reconstruction with a white light, manufacturing large hologram without large collimating system, fine full color hologram etc. as in the case of a conventional analog reflection hologram.

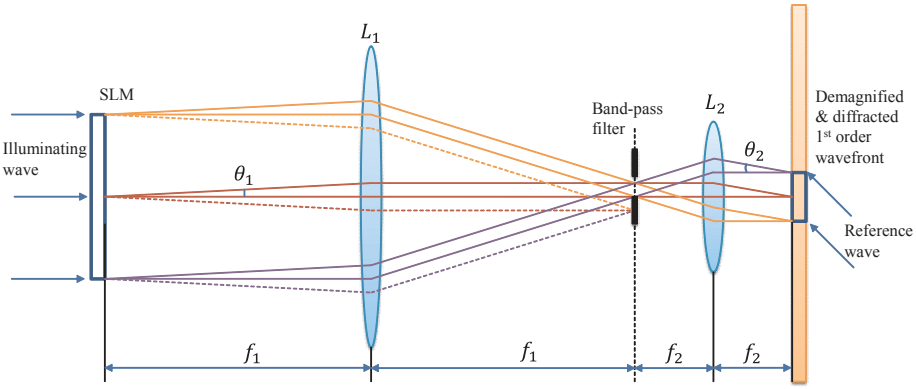

Figure 20. An optical schematic of a wavefront printer.

Below we describe the principle of the proposed by us wavefront printer for production of white-light viewable CGHs. In case of a conventional analog hologram, the scattered wave from a real object propagates to the holographic emulsion and interferes with an illuminating reference wave. The formed interference pattern is recorded as a hologram. In other words, the wavefront coming from the object is recorded onto the holographic emulsion. In the same way, the wavefront from a virtual object, which is generated by computer graphic tools, can be recorded by a wavefront printer. Actually, this is the only printer capable to record a wavefront coming from a virtual object and encoded as a CGH.

An optical schematic of a wavefront printer is shown in Fig. 20. A holographic fringe pattern generated by computer is displayed by a SLM, and an illuminating wave is diffracted by the SLM. The diffracted wave passes through the first lens, L_1. This wave is filtered by a band-pass filter which cuts off the undesired components such as the -1st order diffracted wave and non-diffracted wave. Therefore, only the desired 1st order diffracted wave goes through the filter, and is demagnified by the two lenses, L_1 and L_2. The demagnified wavefront interferes with an illuminating reference wave in a holographic emulsion placed at the focus of the lens L_2. The interference pattern is recorded as a holographic element. The fringe pattern on the SLM is updatable, and the recording location over the holographic emulsion is also changed accordingly. Therefore, the holographic fringe pattern corresponding to different hogel locations is recorded as a volume reflection hologram. Thus, a hologram is formed which encodes the wavefront of light coming from the object. The hologram can be reconstructed under white light illumination.

http://dx.doi.org/10.5772/53412

The hologram can be used also as a master hologram to make a transfer hologram by using the reference wave as that in the recording step for illumination of the whole area of the recorded master hologram as is shown in Figure 21. The holographic emulsion of the second hologram is placed at the location of the reconstructed image. The second hologram is illuminated with a reference wave. After recording of the second hologram, it can be reconstructed under white light illumination. Thus we can see a hologram with a naked eye. The optical reconstruction is shown in Figure 22. A virtual object, the logo of the Korea Electronics Technology Institute, is recorded digitally by the proposed wavefront printing technique, and the obtained hologram reconstructs the image like a conventional analog hologram under illumination with a point light source (a LED).

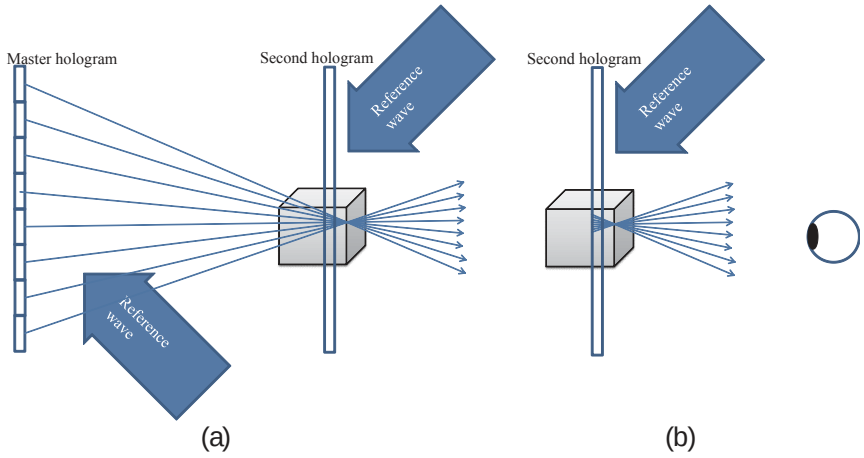

Figure 21. a) Recording schematic for second hologram, (b) holographic display.

Figure 22. The optical reconstruction of the second hologram.

4. Future trends

The holographic printer has the potential to be useful equipment for industry, medicine, cultural heritage protection, commerce and entertainment because of its capability to represent exact 3D space without any distortion and visual fatigues. However, although numerous attractive printed holograms have been created in the recent years, the market is still not populated with holographic printers due to some technical difficulties. There are a lot of unsolved issues which should be overcome. Among them, the most important are the time consuming holographic recording procedure, a rather bulky recording system with extremely high price and quality of the printed hologram. Generally, the frame per second (fps) rate of a conventional SLM is about 30 fps, therefore, a conventional holographic printer is able to record 30 hogels per one second. If a hogel size is 1 mm × 1 mm and a hologram place size is 1 M × 1 M, then the recording procedure will take approximately 10 hours. This issue might be a serious obstacle for market realization. The recording time can be reduced with a tuned mass damper or active vibration control, but this solution also has a limitation. The ultimate solution of the problem by using pulsed laser is, however, very expensive. High-end components such as SLMs with high frame rate, wide angle objectives, lasers with single longitudinal mode, lenses etc. are required to build a holographic printer. Moreover, such optical and electrical components are mounted on a vibration insulated optical table. For industrialization and commercialization, further improvement of the holographic printer is mandatory to facilitate its use in office and conventional places. The final issue is the quality of the printed hologram. In case of a holographic stereogram, multiple perspectives are used as an input data, and angular intensity distributions which are made using the multiple perspectives are recorded onto a holographic emulsion. Because the perspectives already have unwanted distortions from the used optics such as radial distortion, depth distortion etc. the represented 3D space is also distorted. This means that an observer may not be able to experience a true 3D perception even at properly encoded information about the 3D scene. The unsolved issues put a lot of challenges to be overcome in the near future to make the holographic printer a conventional equipment in our everyday life, industry, education, and cultural exchange.

Author details

Hoonjong Kang[1], Elena Stoykova[1,2*], Jiyung Park[1], Sunghee Hong[1] and Youngmin Kim[1]

*Address all correspondence to: e.stoykova@keti.re.kr

1 Broadcasting &ICT R&D Division, Korea Electronics Technology Institute, F8, Sangam-dong, Mapo-gu, Seoul, Korea

2 Institute of Optical Materials and Technologies, Bulgarian Academy of Sciences, Sofia, Bulgaria

http://dx.doi.org/10.5772/53412

References

[1] Gabor D, A new microscopic principle. Nature 1948;161: 777-778.

[2] Schnars U, Jueptner W. Direct recording of holograms by a CCD target and numerical reconstruction Applied Optics 1994; 33(2):179-181.

[3] Kreis T, editor. Handbook of holographic interferometry: Optical and Digital Methods, Wiley-VCH GmbH&Co.KGaA: Weinheim; 2006.

[4] Boyer K, Solem J, Longworth J, Borisov A, Rhodes C. Biomedical three-dimensional holographic microimaging at visible, ultraviolet and x-ray wavelengths, Nature medicine 1996; 2(8): 939-941.

[5] Pole RV. 3-D imagery and holograms of objects illuminated in white light. Applied Physics Letters 1967; 10(1): 20-22.

[6] De Bitetto D. Holographic panoramic stereograms synthesized from white light recordings. Applied Optics 1969; 8(8): 1740–1741.

[7] King M, Noll A, Berry D. A new approach to computer-generated holography. Applied Optics 1970; 9(2): 471-475.

[8] Benton S. Hologram reconstructions with extended incoherent sources. Journal of the Society of America 1969; 59(10): 1545-1546.

[9] Pizzanelli D. The development of direct-write digital holography. Proc. of 'Holography, Art and Design' Conference, Royal College of Art, London. (23 March 2002). http://www.holography.co.uk/events/eventindex.htm

[10] Yatagai T. Three-dimensional display using computer-generated holograms. Optics Communications 1974; 12(1): 43-45.

[11] Yatagai T. Stereoscopic approach to 3-D display using computer-generated holograms. Applied Optics 1976; 15(11): 2722-2729.

[12] Yamaguchi M, Ohyama N, Honda T. Holographic 3-D printer. Proc. SPIE 1990; 1212: 84-92.

[13] Yamaguchi M, Ohyama N, Honda T. Holographic three-dimensional printer: new method. Applied Optics 1992; 31(2): 217-222.

[14] Klug M, Holzbach M, Ferdman A. Method and apparatus for recording 1-step full color full parallax holographic stereograms. U.S. Patent 1998; No.US630088B1.

[15] Brotherton-Ratcliffe D, Vergnes F, Rodin A, Grichine M. Method and apparatus to print holograms. Lithuanian Patent 1999a; No.LT4842.

[16] Brotherton-Ratcliffe D, Vergnes F, Rodin A, Grichine M. Holographic Printer. U.S. Patent 1999b; No. US7800803B2.

[17] Rodin A, Vergnes FM, Brotherton-Ratcliffe D. Pulsed multiple colour laser. EU Patent 1236073; 2001.

[18] Brotherton-Ratcliffe D, Zacharovas S, Bakanas R, Pileckas J, Nikolskij A, Kuchin J. Digital holographic printing using pulsed RGB lasers. Optical Engineering 2011; 50(9): 091307-091307-9.

[19] Blanche PA, Bablumian A, Voorakaranam R, Christenson C, Lin W, Gu T, Flores D, Wang P, Hsieh WY, Kathaperumal M, Rachwal B, Siddiqui O, Thomas J, Norwood RA, Yamamoto M, Peyghambarian N. Holographic three-dimensional telepresence using large-area photorefractive polymer. Nature 2011;468: 80-83.

[20] Hahn J, Kim H, Lim Y, Park G, Lee B. Wide viewing angle dynamic holographic stereogram with a curved array of spatial light modulators. Optic Express 2008; 16(16): 12372-12386.

[21] Yoshikawa H, Takei K. Development of a compact direct fringe printer for computer-generated holograms. Proc. SPIE 2004; 5290: 114-121.

[22] Yoshikawa H, Tachinami M. Development of direct fringe printer for computer-generated holograms. Proc. SPIE 2005; 5742: 259-266.

[23] Benton S. Survey of holographic stereograms. Proc. SPIE 1983; 367: 15-19.

[24] Halle M. Holographic stereograms as discrete imaging systems. Proc. SPIE 1994; 2176: 73-84.

[25] Leith E, Voulgaris P. Multiplex holography: some new methods. Optical Engineering 1985; 24: 171-175.

[26] Aebischer N, Carquille B. White light holographic portraits (still or animated). Applied Optics 1978; 17(23): 3698-3700.

[27] Halle M. The Generalized holographic stereogram. PhD thesis. MIT Dept. of Electrical Engineering and Computer Science, Cambridge MA, USA; 1993.

[28] Halle M, Benton S, Klug M, Underkoffler J. The Ultragram: A Generalized Holographic Stereogram. Proc. SPIE 1991; 1461 "Practical Holography V" (SPIE, Bellingham,WA, February) paper #21

[29] Klug M, Halle M, Hubel P. Full color ultragrams. Proc. 1992; SPIE 1667: 110-119.

[30] Yamaguchi M, Hoshino H, Honda T, Ohyama N. Phase added stereogram: calculation of hologram using computer graphic technique. Proc. SPIE 1993; 1914, 25-33.

[31] Smithwick Q, Barabas J, Smalley D, Bove V. Interactive holographic stereograms with accommodation cues. Proc. SPIE 2010; 7619: 761903-1-761903-13.

[32] Lucente M. Diffraction-Specific Fringe Computation for Electro-Holography. PhD thesis, MIT Dept. of Electrical Engineering and Computer Science, Cambridge MA; 1994.

[33] Honda T, Yamaguchi M, Kang D.-K, Shimura K, Tsujiuchi J, Ohyama N. Printing of holographic stereograms using liquid-crystal TV. Proc. SPIE 1989; 1051: 186-191.

[34] Benton S. Real Image Holographic Stereograms. U.S. Patent 4834476 (issued 30 May 1989).

[35] Zacharovas S. Advances in digital holography. In: Proceedings of the International Workshop on Holographic Memories, IWHM2008, 20-23 October 2008, Aichi, Japan; 55-67.

[36] Klug M, Halle M, Lucente M, Plesniak W. A compact prototype one-step ultragram printer. Proc. SPIE 1993; 1914: 15-23.

[37] Hellseth L, Singstad I. Diffusers for holographic stereography. Optics Communications 2001; 193(1): 81-86.

[38] Bjelkhagen H, Mirlis E. Color holography to produce highly realistic three-dimensional images. Applied Optics 2008; 47(4): A123-A133.

[39] Yamaguchi M, Honda T, Ohyama N, Ishikawa J. Multidot recording of rainbow and multicolor holographic stereograms. Optics Communications 1994; 110 (5-6): 523-528.

[40] Yamaguchi M, Koyama T, Ohyama N, Honda T. A stereographic display using a reflection holographic screen. Optical Review 1994; 1(2): 191-194.

[41] Yamaguchi M, Endoh H, Honda T, Ohyama N. High quality recording of a full-parallax holographic stereogram with a digital diffuser. Optics Letters 1994; 19(2): 135-137.

[42] Zebra Imaging Inc. Company (2012) http://www.zebraimaging.com/.

[43] 3D Holoprint. Company (2012) http://www.3d-holoprint.com/.

[44] Yamaguchi M, Sugiura H, Honda T, Ohyama N. Automatic recording method for holographic three-dimensional animation. Journal of the Optical Society of America A 1992; 9(7): 1200-1205.

[45] Takano M, Shigeta H, Nishihara T, Yamaguchi M, Takahashi S, Ohyama N, Kobayashi A, Iwata F. Fullcolor holographic 3D printer. Proc. SPIE 2003; 5005: 126-136.

[46] Frey S, Thelen A, Hirsch S, Hering P. Generation of digital textured surface models from hologram recordings. Applied Optics 2007; 46(11): 1986-1993.

[47] Yang F, Murakami Y, Yamaguchi M. Digital color management in full-color holographic three-dimensional printer. Applied Optics 2012; 51(19): 4343-4352.

[48] Yamaguchi M, Endoh H, Koyama T, Ohyama N. High-speed recording of full-parallax holographic stereograms by a parallel exposure systems. Optical Engineering 1996; 35(6): 1556-1559.

[49] Brotherton-Ratcliffe D, Nikolskij A, Zacharovas S, Pileckas J, Bakanas R. Image capture system for a digital holographic printer. U.S. Patent 2009; No.US20090147072A1.

[50] Okada K, Honda T, Tsujiuchi J. A method of distortion compensation of multiplex holograms. Optics Communications 1983; 48(3): 167-170.

[51] Hilaire P. Optimum sampling parameters for generalized holographic stereograms. Proc. SPIE 1993; 3011: 96-104.

[52] Hilaire P. Modulation transfer function and optimum sampling of holographic stereograms. Applied Optics 1994; 33(5): 768-774.

[53] Maruyama S, Ono Y, Yamaguchi M. High-density recording of full-color full-parallax holographic stereogram. Proc. SPIE 2008; 6912: 12-22.

[54] Zacharovas S, Nikolskij A, Kuchin J. DYI digital holography. Proc. SPIE 2011; 7957:79570A-79570A-5.

[55] Sainov S, Stoykova E. Display holography – status and future. In: Osten W, Reingand N. (eds.) Optical Imaging and Metrology. Advanced Technologies, Wiley-VCH; 2012. p 93-115.

[56] Zacharovas S, Rodin A, Ratcliffe D, Vergnes F. Holographic materials available from Geola. Proc.SPIE 2001; 4296: 206-212.

[57] Gentet Y, Gentet P. "Ultimate" emulsion and its applications: a laboratory-made silver halide emulsion of optimized quality for monochromatic pulsed and full-color holography. Proc. SPIE 2000; 4149: 56-62.

[58] Plesniak W, Halle M, Bove V, Barabas J, Pappu R. Reconfigurable Image Projection Holograms. Optical Engineering 2006; 45(11): 115801-1-115801-15.

[59] Yoshikawa H. Computer-generated holograms for white light reconstruction. In: Ting-Chung Poon (ed.) Digital Holography and Three-dimensional Display: Principles and Applications. Springer Verlag; 2006. part 2, p235-255.

[60] Yoshikawa H, Yamaguchi T. Computer-generated holograms for 3D display. Chinese Optics Letters 2009; 7(12): 1079-1082.

[61] Yamaguchi T, Fujii T, Yoshikawa H. Fast calculation method for computer-generated cylindrical holograms. Applied Optics 2008; 47(19): D63-D70.

[62] Yamaguchi T, Fujii T, Yoshikawa H. Computer-generated cylindrical rainbow hologram, Proc. SPIE 2008a; 6912: 69121C-1-69121C-10.

[63] Yamaguchi T, Fujii T, Yoshikawa H. Disk hologram made from a computer-generated hologram. Applied Optics 2009; 48(34): H16-H22.

[64] Yamaguchi T, Yoshikawa H. Computer-generated image hologram. Chinese Optics Letters 2011; 9(12): 120006.

[65] Yoshikawa H, Yamaguchi T, Kitayama R. Real-time generation of full color image hologram with compact distance look-up table. In: Digital Holography and Three-Dimensional Imaging, April 30, 2009, Vancouver, Canada; DWC4.

[66] Fujii T, Yoshikawa H. Improvement of Hidden-Surface Removal for Computer-Generated Holograms from CG. In: Digital Holography and Three-Dimensional Imaging, June 18, 2007, Vancouver, Canada; DWB3.

[67] Kang H, Yamaguchi T, Yoshikawa H. Processing techniques for quality improvement of phase added stereogram. Proc. SPIE 2007; 6488: 6488-41.

[68] Kang H, Fujii T, Yamaguchi T, Yoshikawa H. A Compensated Phase-Added Stereogram for Real-Time Holographic Display. Optical Engineering 2007; 46 (9): 095802-1-095802-11.

[69] Kang H, Yamaguchi T, Yoshikawa H. Accurate phase-added stereogram to improve the coherent stereogram. Applied Optics 2008; 47(19): D44-D54.

[70] Kang H, Yamaguchi T, Yoshikawa H. Accurate phase-added stereogram. In: Digital Holography and Three-Dimensional Imaging, June 18, 2007, Vancouver, Canada; DTuB5.

[71] Kang H, Yamaguchi T, Yoshikawa H, Kim SC, Kim ES. Acceleration method of computing a compensated phase-added stereogram on a graphic processing unit. Applied Optics 2008; 47(31): 5784-5789.

[72] Lee A. Computer-generated hologram recording using a laser printer. Applied Optics 1987; 26(1): 136-138.

[73] Yatagai T, Camacho-Basilio J, Onda H. Recording of computer-generated holograms on an optical disk master. Applied Optics 1989; 28(6): 1042-1044.

[74] Cable A, Mash P, Wilkinson T. Production of computer-generated holograms on recordable compact disk media using a compact disk writer. Optical Engineering 2003; 42(9): 2514-2529.

[75] Sakamoto Y, Morishima M, Usui A. Computer generated holograms on a CD-R disk. Proc. SPIE 2004; 5290: 42-49.

[76] Matsushima K, Kobayashi S, Miyauchi H. A high-resolution fringe printer for studying synthetic holograms. Proc. SPIE 2006; 6136: 347-354.

[77] Yamaguchi T, Maeno Y, Fujii T, Yoshikawa H. Animated computer-generated cylindrical hologram. NICOGRAPH International 2008. [CD-ROM].

[78] Miyamoto O, Yamaguchi T, Yoshikawa H. The volume hologram printer to record the wavefront of a 3D object. Proc. SPIE 2012; 8281: 82810N-82810N-10.